Science of the Total Environment 512–513 (2015) 345–352

Contents lists available at ScienceDirect

Science of the Total Environment

journal homepage: www.elsevier.com/locate/scitotenv

$nTiO_2$ induced changes in intracellular composition and nutrient stoichiometry in primary producer — cyanobacteria

Carla Cherchi [a], Milos Miljkovic [b], Max Diem [b], April Z. Gu [a,*]

[a] Department of Civil & Environmental Engineering, 360 Huntington Avenue, Northeastern University, Boston, MA 02115, USA
[b] Department of Chemistry and Chemical Biology, 360 Huntington Avenue, Northeastern University, Boston, MA 02115, USA

HIGHLIGHTS

- Exposure to $nTiO_2$ induced changes in cell composition and intracellular nutrient element ratios.
- $nTiO_2$ exposure led to both temporal and dose-dependent change patterns of major macromolecules
- Physiological cellular changes in Cyanobacteria suggest ecological implications of $nTiO_2$ exposure

GRAPHICAL ABSTRACT

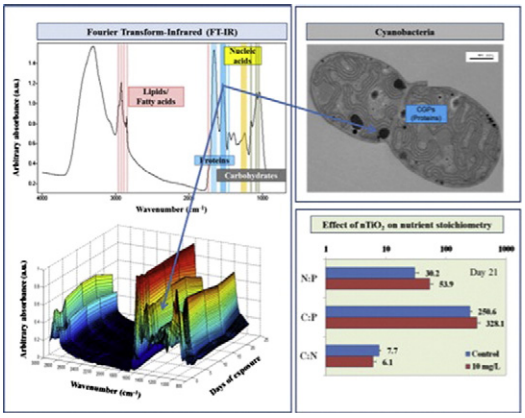

ARTICLE INFO

Article history:
Received 18 June 2014
Received in revised form 31 December 2014
Accepted 15 January 2015
Available online 27 January 2015

Editor: Kevin V. Thomas

Keywords:
Nano-titanium dioxide
Ecotoxicity
Algae
Anabaena variabilis
FT-IR
Nutrients

ABSTRACT

The widely and increasing use of nano-titanium dioxide ($nTiO_2$) has led to its release in the environment and concerns of consequent impact on aquatic eco-relevant biota. Previous studies indicated possible physiological changes (i.e., nitrogen storage) induced by nano-titanium dioxide ($nTiO_2$) exposure in algae, which will likely have ecological implications. This study investigated the short- (96 h) and long-term (21 days) ecotoxic impact of environmentally relevant $nTiO_2$ concentrations on the cellular biochemical pools and nutrient stoichiometry in the nitrogen-fixing cyanobacteria *Anabaena variabilis*. Changes in nutrient element ratios and cellular composition were analyzed using both chemical elemental analysis and Fourier Transform Infrared (FT-IR) spectroscopy. Chemical elemental analysis showed that exposure to $nTiO_2$ at varying dose concentrations and exposure duration led to statistically significant changes in intracellular C:N, C:P and N:P stoichiometries compared with those in the controls. In general, there seemed to be a decreasing trends of cellular C:N ratio and increase in the cellular C:P and N:P ratios with the increasing level of $nTiO_2$ exposure. Further FT-IR analysis results revealed both temporal and dose-dependent change patterns of major macromolecules, including protein, lipids, nucleic acids and carbohydrates, in *A. variabilis* upon $nTiO_2$ exposure. The relative ratio of amide II, lipids, nucleic acids and carbohydrates to the cellular protein content (quantified as amide I stretch) changed significantly within the initial 96 h of exposure and, both the magnitude of changes and levels of recovery seemed to be $nTiO_2$ dose-dependent. This study, for the first time, demonstrated that the intracellular composition and nutrient

* Corresponding author.
E-mail address: april@coe.neu.edu (A.Z. Gu).

http://dx.doi.org/10.1016/j.scitotenv.2015.01.037
0048-9697/

stoichiometry changes could be induced by long-term and short-term exposures to $nTiO_2$ to primary producers, which may have ecological implications for interspecies equilibriums and community dynamics in aquatic ecosystems.

1. Introduction

Progress of nanotechnology poses an urgent need for fundamental understanding of the potential environmental impacts of engineered nanomaterials (NMs). Nanosize titanium dioxide ($nTiO_2$) has a wide range of applications because of its excellent electrical properties and optical performances (Chen et al., 2009). Its presence in wastewater effluents has been anticipated (Mueller and Nowack, 2008), recently evidenced (Kiser et al., 2009) and it will likely impact aquatic biota and eco-relevant organisms. In particular, the toxic effect of $nTiO_2$ on algal species and on ecosystems is still largely unexplored.

Previous literature have reported geno- and cyto-toxic effect of $nTiO_2$ on human cell lines and bacteria (Wang et al., 2007; Gou et al., 2010; Xu et al., 2009), indicating that DNA damage (Jha et al., 2008), membrane disruption (Wiesner and Bottero, 2007) and protein oxidation via reactive oxygen species formation (Neal, 2008) are the major mechanisms of toxicity involved. Recent studies investigated $nTiO_2$ impact on algal ecosystems, showing deleterious effects on algal growth (Lin et al., 2012; Ji et al., 2011) and photosynthetic and nitrogen-fixing activities (Ji et al., 2011; Miller et al., 2010; Cherchi and Gu, 2010; Aruoja et al., 2009; Sharma, 2009; Wang et al., 2008). However, studies on long-term impact on cellular physiological changes at environmentally relevant low exposure concentrations have been scarce. Our previous study revealed that cell topology, mechanical properties and intracellular structures of cyanobacteria were compromised after exposure to $nTiO_2$ (Cherchi et al., 2011). Particularly, the dose-dependent accumulation of the nitrogen storage polymer (cyanophycin grana proteins, CGPs) in the cyanobacteria *Anabaena variabilis* in response to $nTiO_2$ treatments was demonstrated, which indicated that the intracellular nutrient metabolism and stoichiometry may be potentially modified by the exposure to $nTiO_2$ (Cherchi and Gu, 2010). The implications of C:P and N:P variations are well-documented, although not fully elucidated, known to impair biologically mediated flows of energy and nutrients in ecosystems and modify organisms' sensitivity to external nutrients (Elser, 2006).

To further investigate the toxicity impact of $nTiO_2$ to essential macromolecular cell components linked to specific cell functions and metabolism and consequently to the intracellular nutrient stoichiometry, in the present study, we evaluated the effects of $nTiO_2$ exposure at sub-lethal environmental relevant concentrations on the cellular allocation of macromolecules (nucleic acids, proteins, lipids, carbohydrates) in the cyanobacteria *A. variabilis*. Cyanobacteria are of significant biogeochemical importance due to their contribution to primary productivity and their ability to tolerate adverse and fluctuating environmental stresses by implementing unique metabolic strategies (Apte et al., 1998). Microalgae are known for their ability to carry a dramatic reorganization of internal macromolecules and therefore, of their nutrient status, when overcoming abiotic stress conditions (Patel et al., 2008; Giordano et al., 2001). Previous studies have reported such responses in algal ecosystems exposed to toxicants, such as the decrease in protein content in the algae *Micrasterias hardyi* after contact with active pharmaceutical ingredients (Patel et al., 2008) and the decrease in energy storage products (i.e., carbohydrates) in the brown algae *Padina tetrastromatica* under stress induced by cadmium (D'Souza et al., 2008). Alterations in the relative presence of carboxyl, phosphoryl, hydroxyl, and amine functional groups will generate variations not only at the single cell level (i.e., homeostatic regulation processes) but also at larger scale with modifications on cell growth, fitness, interspecies relationship, trophic interactions and food web dynamics (Levin, 2009).

In this study, a quantitative elemental analysis was performed to demonstrate $nTiO_2$-induced deviations of intracellular nutrient stoichiometry from those of cells in control (untreated) conditions. In addition, cellular composition fingerprinting obtained with the analysis of spectral signatures using FT-IR, as well as chemometric methods, revealed high-resolution temporal change patterns of major biochemical pools and chemical markers upon short- (96 h) and long-term (21 days) exposure to different doses of $nTiO_2$. The results provided important insights into the impact of $nTiO_2$ exposure on intracellular composition and stoichiometry and revealed potential ecological implications of long-term NM exposure.

2. Experimental methods

2.1. NM preparation and characterization

Nano-TiO_2 anatase ($nTiO_2$, primary size 10 nm, NanoStructured & Amorphous Materials, Houston, Texas, USA) was prepared in a modified Mes-Volvox medium (Cherchi et al., 2011) and then dispersed via sonication in a High energy Cup-sonicator (Fisher scientific, Inc.), at ~90 Watt power for 20 min. Bovine Serum Albumin (1% BSA) was added in the stock solution (10 g-$nTiO_2$/L) to enhance the dispersion for uniform dosing (Pal et al., 2011). Physical and chemical characterization of $nTiO_2$ was detailed in previous studies (Cherchi and Gu, 2010; Bello et al., 2008) and is also shown in STable 1. Detailed physical and chemical characterization of the $nTiO_2$ used in this study, including aggregate size distribution, metal impurities, surface charge, zeta potential, organic and elemental carbon etc., was conducted and reported by Bello et al. Primary size $nTiO_2$ from manufacturer was 10 nm (outer diameter) and the average size of NM aggregates of 192 ± 0.8 nm was determined through Dynamic Light Scattering (Zetasizer Nano ZS90, Malvern Instruments Ltd.) after NM dispersion in the culture media (single crystal). The polydispersity index (PdI) after dispersion in culture media was found to be 0.479. A specific surface area of 274.2 $m^2\ g^{-1}$ was measured and the X-ray diffraction showed the presence of small amount of both anatase and rutile soluble extracts in the $nTiO_2$ anatase used in this study (Bello et al.). Transmission electron microscopy was used to observe $nTiO_2$ behavior during ecotoxicological tests of exposed *Anabaena* cells. From the analysis of 115 aggregates observed across samples exposed for to 24 and 96 h to 1 mg/L to 150 mg/L, $nTiO_2$ agglomerates of average 435.0 nm ± 275.5 nm (longest dimension) were observed (STable 1).

2.2. Culture conditions and ecotoxicological tests

A. variabilis strain (UTEX #1444), also referred to as *Trichormus variabilis*, was cultured in a modified Mes-Volvox media, with conditions described in our previous work (Cherchi and Gu, 2010). For exposure tests, 500 mL batch reactors of initial chlorophyll *a* concentration of 200 μg/L were dosed with different $nTiO_2$ concentrations, ranging from 0 mg-$nTiO_2$/L (control sample) to 1 mg-$nTiO_2$/L, and incubated for 21 days under a 12 h light/12 h dark regime to mimic natural environmental conditions. The light source used 1:1 ratio of 34 W cool white and 40 W gro-lux fluorescent bulbs (Sylvania, Danvers) of wavelength output >400 nm, which yields a low PAR value of 35 μ mol photon/$m^2 \cdot s$. Batches were continuously mixed (300 rpm) and aeration was continuously provided via 0.2 μm filtered compressed air to deliver air in the reactors' headspace at a rate of 5 mL/min. Chlorophyll *a* has often served as indicator for algal growth assessment

(Geis et al., 2000) and our previous studies (STable 2) showed that chlorophyll *a* correlated well with cell count of *A. variabilis* and, therefore, was employed as a surrogate to measure growth in this study. Chlorophyll *a* was measured by fluorescence after ethanol extraction by a Synergy HT fluorometer (BioTek, Winooski, VT) with excitation and emission at 440 nm and 670 nm, respectively. Algal growth inhibition tests based on chlorophyll *a* measurements were performed according to standard protocols (U.S. Environmental Protection Agency, 2002). Chlorophyll *a* measurements of growth showed exponential and continued growth over the duration of the experiment (21 days) for all treated and untreated cultures (data not shown) and stationary conditions were not reached during the 21 day assay. Batch tests were performed in duplicates and all measurements were conducted in triplicates. Total cellular proteins were assayed colorimetrically on sonicated cells (75 W, 60 s), with a bicinchoninic acid (BCA) protein assay kit (Pierce Chemical Co., Rockford, IL) and standards prepared with BSA. Interferences of BSA introduced from $nTiO_2$ stock solution preparation were measured to be negligible (lower than detection limit). All protein measurements were performed in triplicates.

2.3. Chemical elemental analysis of intracellular macronutrients

An independent experiment was performed to determine the intracellular elemental nutrients in *A. variabilis*' cells exposed to $nTiO_2$ concentrations of 1, 10 and 100 μg/L and 1 and 10 mg/L for 96 hour and 21 day exposures. Exposure condition was similar to those ecotoxicity assays described previously and all tests were run in triplicate batches. Elemental carbon and nitrogen analysis was performed on pre-washed and overnight freeze-dried samples containing 1–3 mg of biomass, and measured using a CE-440 elemental analyzer (Exeter Analytical, Inc., Chelmsford, MA). Combustion was obtained at 950 °C in the presence of ultrapure oxygen and CO_2, H_2O and N_2 were detected by thermal conductivity analyzer. Final concentrations of C, H, and N in the samples were expressed as percentage of the elements per unit mass of the freeze-dried samples. Intracellular levels of phosphorus were determined on pre-washed and oxalate-treated cells, following acid hydrolysis by the persulfate digestion method and measured via spectrophotometric analysis (Shimadzu, Columbia, MD), according to previous methods (American Public Health Association, 1999). All elemental analysis was performed in triplicates. Pairwise Student's t-test was used to assess statistical significance of the obtained results.

2.4. FT-IR spectroscopy analysis of cell components

Aliquots of sample (20 mL) were periodically withdrawn and cells were fixed in Lugol's iodine solution (1 μL/mL) followed by resuspension in deionized water. An aliquot (4 μL) of the cell suspension was transferred onto a MirrIR low-e reflectance microscopic slides (Kevley Technologies, Chesterland, USA), desiccated under vacuum before analysis. Spectra were collected using a Perkin Elmer Spectrum One Fourier Transform Infrared (FT-IR) spectrometer bench coupled to a Spotlight 300/400 IR microscope, fitted with a liquid N_2 cooled mercury–cadmium–tellurium detector (PerkinElmer Inc., Shelton, CT, USA). Absorbance spectra were collected in point scan mode at a spectral resolution of 4 cm^{-1} with 20–64 scans co-added and averaged on 25 μm^2 randomly selected areas of deposed cells. At least 60 to 80 spectra (Heraud et al., 2008) in the wavenumber region between 750 and 4000 cm^{-1} were recorded for each sample, yielding a total of >6000 spectra analyzed. Band assignment is based on previous studies (Giordano et al., 2001; Murdock and Wetzel, 2009; Kansiz et al., 1999) and is summarized in STable 3.

2.5. Principal component analysis

FT-IR spectra were imported into Matlab v. 7.8.0 (R2009a), where surface fitting and data analysis were carried out using the PLS toolbox (Eigenvector Technologies, Manson, USA). To reduce the potential bias associated with the spectra baseline, baseline correction was performed and spectra were pre-processed using the maximum normalization algorithm which normalizes to the most intense frequency in the spectrum (amide I). For the analysis, first derivatives of the corrected spectra were computed using the Savitsky and Golay algorithm with an 11 point window and a third order polynomial fitting. Data were then mean centered before being subjected to the PLS toolbox for principal component analysis (PCA). Principal components (PCs) were calculated and PCA score plots were used to visualize any clustering of the samples. Loading plots were used to determine the spectral region that contributed the most to the variance in the dataset.

3. Results and discussions

3.1. Nano-TiO_2 exposure impact on intracellular element stoichiometry

To test the hypothesis that the $nTiO_2$ exposure may induce cellular changes in composition and macromolecule pools, we evaluated the intracellular nutrient element balances and stoichiometry of *A. variabilis* upon $nTiO_2$ exposure at 96 h and 21 days with varying dose concentrations ranging from 1 μg-$nTiO_2$/L to 10 mg-$nTiO_2$/L. Elemental quantitative analysis (Table 1) shows impact of $nTiO_2$ exposure on intracellular nutrient stoichiometry (C:N, C:P, N:P) at varying dose concentrations (including untreated controls), and with different exposure time lengths (96 h versus 21 days). In the controls without $nTiO_2$ exposure, the cellular C:N ratio showed a 5.6% decrease after 96 h of culture, and a 4.5% increase after 21 day exposure. However, both C:P and N:P ratios in the controls showed slight increase compared to initial measurements at time zero. This biochemical variability at various phases of growth has been previously reported on various aquatic species, including green algae (Sigee et al., 2007; Liang et al., 2006), and likely linked to changes in the extent of carbon and nitrogen fixation of cells when approaching late exponential growth conditions (Mulholland and Capone, 2001). Note that the exposure of *A. variabilis* cultures to $nTiO_2$ at environmentally relevant low concentrations (1–1000 μg/L) did not lead to any observable growth inhibition (based on chlorophyll *a*) with short-term exposure (96 h) (data not shown); however, growth inhibition of 6.5 ± 0.7% ($p = 0.03$) was detected with long-term exposure (21 days) at 1 mg/L (SFig. 1). This is consistent with our previous report of the CT (concentration (C) and exposure time (T))-dependent toxicity of $nTiO_2$ (Cherchi and Gu, 2010).

Exposure to $nTiO_2$ at varying dose concentrations and exposure durations led to statistically significant changes in intracellular C:N:P

Table 1
Elemental intracellular ratios of C:N, C:P and N:P (on a % dry mass basis) for *A. variabilis* exposed to $nTiO_2$ concentrations (1, 10, 100 μg/L and 1, 10 mg/L) for 96 h and 21 days. Average and standard deviations are of 3 independent experiments.

	C:N	C:P	N:P
Time − 0			
Control	7.4 ± 1.4	143.3 ± 1.61	19.9 ± 4.0
10 mg/L	7.5 ± 0.1	155.3 ± 19.2	20.7 ± 2.6
Time − 96 h			
Control	6.9 ± 0.1	292.6 ± 17.0	42.1 ± 2.8
1 μg/L	7.0 ± 0.5	235.0 ± 79.3	32.0 ± 6.6
10 μg/L	–	–	–
100 μg/L	6.5 ± 0.3	421.2 ± 50.6*	64.2 ± 4.9*
1 mg/L	6.3 ± 0.2*	347.4 ± 31.7	55.4 ± 6.5*
10 mg/L	7.4 ± 0.3*	327.9 ± 10.9	43.5 ± 0.1
Time − 21 days			
Control	7.7 ± 0.4	250.6 ± 17.1	30.2 ± 4.5
1 μg/L	7.1 ± 0.1	367.7 ± 32.8*	51.5 ± 4.2*
10 μg/L	6.5 ± 0.4*	195.3 ± 31.8	30.2 ± 6.4
100 μg/L	7.3 ± 0.3	294.1 ± 43.2	40.4 ± 7.9
1 mg/L	7.3 ± 0.3	309.3 ± 50.6	42.3 ± 6.7
10 mg/L	6.1 ± 0.7*	328.1 ± 38.4*	53.9 ± 6.4*

* Statistically significant values based on Student's t-test at $p < 0.05$.

stoichiometry compared with those in the controls (Table 1). Potential interferences of $nTiO_2$ on chemical elemental analysis were excluded, since the C:N, C:P and N:P ratios of the control were consistent and comparable to those at 10 mg-$nTiO_2$/L at initial time zero. Both short-term exposure and long-term exposure to $nTiO_2$ led to statistically significant changes in the cellular C:N, C:P and N:P ratios. Trends of elemental ratios are found to be dose-specific, indicating that different doses can trigger different biochemical responses and cell behaviors at various exposure time lengths. In general, there seemed to be decreasing trends of cellular C:N ratio and increase in the cellular C:P and N:P ratios with the increasing level of $nTiO_2$ exposure. For example, at 21 day-exposure study, exposed cells mostly exhibited a general decrease in C:N, as much as 21% compared to the control, and concurrent increase in C:P and N:P ratios, by up to 31% and 77% respectively, for exposure at 10 mg-$nTiO_2$/L ($p < 0.05$).

These results clearly demonstrate that $nTiO_2$ exposure induces alterations in the intracellular C:P and N:P ratios in comparison to controls without $nTiO_2$ exposure. The implications of C:P and N:P variations upon conditions of stress are well-documented, although not fully elucidated, and certainly known to impair biologically mediated flows of energy and nutrients in ecosystems and modify organisms' sensitivity to external nutrients, thus ecological nutrients cycling (Elser, 2006). Algal species composition regulates cell growth and affects food webs at all levels, therefore influencing their ability to meet their reproductive and nutritional requirements (Glibert, 2012). For example, previous study have suggested that lower molar C:N ratio (<10) of the microalgae *Rhodomonas* sp. resulted in a lower egg production in the copepod *Acartia* sp. (often used as bio-indicators) than those fed with microalgae with higher cellular C:N ratio of 10–15 (Augustin and Boersma, 2006). Others have shown that algae with both phosphorus and nitrogen limitation may alter the thickness of their cell wall, making them more resistant to zooplankton digestion than algae with balanced nutrient conditions (Schwarzenberger et al., 2013). In addition, production of toxins in algae, which are known to impair higher trophic organisms, for example, often occurs when disproportion of internal nutrient stoichiometry exists (Glibert, 2012). Based on these observations, toxicity responses of primary producers to $nTiO_2$ exposure, such as change in intracellular stoichiometry, carbohydrate and lipid relative composition (shown in this study), as well as the increase in N storage cyanophycin and alterations of cell membrane thickness as reported in our previous studies (Cherchi and Gu, 2010; Cherchi et al., 2011) may likely lead to changes in species competition, and consequent implications and impact on aquatic ecosystems.

3.2. Short- and long-term changes in cellular proteins upon $nTiO_2$ exposure

The measured changes in the intracellular elemental nutrient ratios in algal cells motivate further investigation into the underlying causal factors and mechanisms. Increase in proteins has been considered as one of the mechanisms implemented by cells under conditions of stress (Fernandes et al., 1993), and, therefore temporal changes in protein level were firstly evaluated during the $nTiO_2$ exposure assays.

Monitoring of the cell protein content showed cellular protein increase within short-time exposure to $nTiO_2$, as reflected in the changes in the protein/chlorophyll *a* ratios over time (Fig. 1). The protein/chlorophyll *a* ratio for the control remained relatively consistent during the entire test period of 21 days (average of 80 ± 10, similar to previous reported values (10–80) for *Anabaena cylindrica* and *Anabaena doliolum*) (Eisbrenner et al., 1978; Rai and Abraham, 1993), however statistically significant ($p < 0.06$) increase of the protein to chlorophyll *a* ratio was observed for dose concentrations higher than 100 μg-$nTiO_2$/L (Table 2). The $nTiO_2$-induced high cellular protein content then decreased in the following four days and reached a relatively stable level in the long-term period. Although the underlying mechanisms of this temporal protein elevation is not clear, changes in the ratio are possibly related to perturbation in protein synthesis and its structures caused by abiotic stresses, as the increase in proteins (i.e., stress response proteins) has been reported to be part of the stress response mechanism within cells (Fernandes et al., 1993).

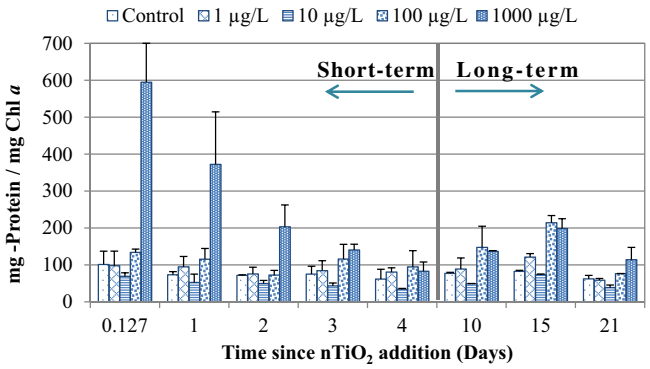

Fig. 1. Average protein/chlorophyll *a* ratio in *A. variabilis* cells after exposure to different $nTiO_2$ concentrations ranging from 0 to 1000 μg/L, during short-term (96 h) and long-term (21 days) exposures. Standard deviations shown are calculated from biological duplicate experiments (n = 2) with triplicate measurements of chlorophyll *a* and protein for each sample collected.

3.3. Dose-dependent changes in cellular structure and composition of *A. variabilis* upon $nTiO_2$ exposure

To gain further insights into the effects of $nTiO_2$ exposure at sub-lethal environmentally relevant concentrations on the cellular allocation of macromolecules (nucleic acids, proteins, lipids, carbohydrates) in the cyanobacteria *A. variabilis* and consequently the intracellular element stoichiometric ratios, we further applied FT-IR to monitor the physiological state of *A. variabilis* cells and the results revealed structural changes and reallocation of intracellular pools in response to $nTiO_2$ exposure at various concentrations. SFig. 2 shows the example of temporal changes in the FT-IR spectra of the culture exposed to 1000 μg-$nTiO_2$/L compared to the control with no NM exposure. Two protein signatures, namely amide I and amide II, are interpreted from the most prominent stretching at 1650 cm^{-1} (C=O stretch), typical of α-helical and parallel β-sheets of random coiled protein structures, and the in-plane N–H bending of amides (1540 cm^{-1}), respectively. Antisymmetric C–H markers at 2920 cm^{-1} and 2956 cm^{-1} and symmetric stretching at 2852 cm^{-1} and 2876 cm^{-1} are typical of lipids and fatty acids. Insoluble glucose polymers and polysaccharides (e.g., glycogen) exhibit a series of absorption bands due to C–O stretching and C–O–C deformations at 1150 cm^{-1} and 1032 cm^{-1}, respectively. Nucleic acids and phosphorylated molecules have functional groups with absorption bands in the same region of the carbohydrate spectrum, with major asymmetric and symmetric vibrations associated at 1078 cm^{-1} and 1240 cm^{-1}, representing the asymmetric PO_2^- stretch of DNA/RNA backbones, phosphorylated proteins and polyphosphate storage products (Pal et al., 2011). All spectra were normalized to the strongest amide I band and the ratios indicated certain carbon balance within the cell as suggested by Sigee et al. (2007).

A mean centered principal component analysis (PCA) on derivatized spectra was employed to classify *A. variabilis* response as a function of $nTiO_2$ dose and to examine differences between spectra as a function of exposure time length. The score plots (Fig. 2) project the spectral data onto two principal components (PC1 vs. PC2) and help visualizing

Table 2
p-Value (t-test) of statistical significance for the changes in protein/chlorophyll *a* ratio of exposed samples compared to the control for different exposure time lengths.

	p-Value (t-test)			
	1 μg/L	10 μg/L	100 μg/L	1000 μg/L
Over 21 day exposure	0.14	0.00	0.02	0.02
Over 96 hour exposure	0.23	0.02	0.04	0.06

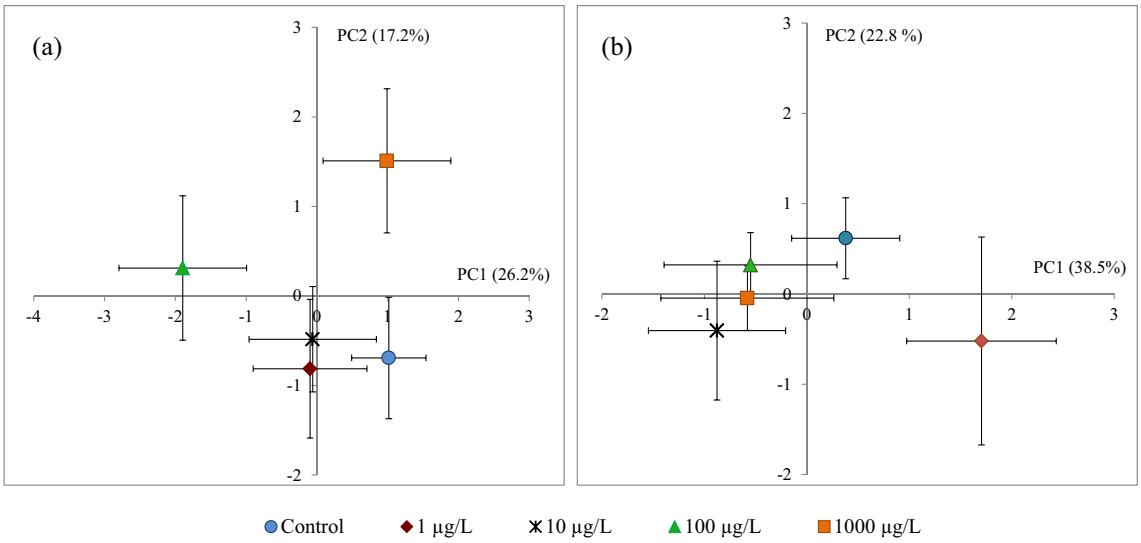

Fig. 2. Score plots on PC1 and PC2 from principal component analysis performed over the region (3000–2700 cm^{-1}; 1800–750 cm^{-1}) of FT-IR spectra obtained from samples exposed to $nTiO_2$ concentrations ranging from 1 to 1000 µg/L for 96 h (a) and 21 days (b). Each point represents the mean PC score for each treatment calculated on 120–160 spectra (60–80 spectra for each), and error bars are the standard error of the mean along the principal component axes.

the degree of separation among the conditions tested. Loading plots (Fig. 3) help to reveal the specific regions of the spectrum (frequencies) that contribute to the variation within the set of data.

The score plots of the PCA performed on both 96 hour and 21 day exposure times show a clear shifting of the mean PC scores associated to different doses of $nTiO_2$ treatment in respect with the mean PC score of the unexposed class, and the separation is distinctive for each exposure time analyzed. Particularly, in the short term (96 h), samples treated with 1, 10 and 100 µg-$nTiO_2$/L show some degree of separation from the control along PC1, with the 100 µg-$nTiO_2$/L class diverging towards the positive PC2, whereas the variation caused by the highest exposure concentration (1000 µg-$nTiO_2$/L) only extends along the PC2. The loading plots showed that the separation observed for cells exposed to 1 and 10 µg-$nTiO_2$/L can potentially be attributed to differences in the symmetric stretches of methyl and methylene groups in fatty acids and methyl groups of lipids (2876 cm^{-1}) and to phosphodiester backbone of nucleic acids (ν_{as} P=O). In addition, differences in intracellular carbohydrate components (ν C–O–C, ν C–O) contribute to the shift in the 100 µgTiO_2/L class. Positive PC1 and PC2 scores for the 1000 µgTiO_2/L class suggest that, in the short period, this exposure concentration induces an array of effects in *A. variabilis* cell, which include changes in symmetric and asymmetric stretches of lipids (2852 cm^{-1}, 2920 cm^{-1} and 2956 cm^{-1}), polysaccharides (ν C–O–C), nucleic acids (ν P=O) and amide (II) groups associated to proteins (δ N–H, ν C–N).

In the long term exposure scenario (21 days), the classification obtained was different from that observed after only 96 h. Interestingly the sample exposed to the lowest concentration (1 µg-$nTiO_2$/L) seems to be the farthest from the control, possibly due to changes in protein stretches (δ N–H, ν C–N and ν C=O) and symmetric CH_2 and CH_3 groups associated to lipids. A very similar long-term response was instead obtained in cells exposed to $nTiO_2$ concentrations ranging from 10 to 1000 µg/L, where the visible stretching along the negative PC1 again reflects a more comprehensive biochemical damage of cytoplasmic components, such as nucleic acids (ν P=O) and polysaccharides (ν C–O–C, ν C–O), and membrane characteristic groups (ν CH_3, ν CH_2, ν_{as} CH_2 and ν_{as} CH_3 of lipids).

From the results of principal component analysis, it is evident the ability of $nTiO_2$ to target *A. variabilis*' cellular components and induce a set of molecular modifications in a dose-dependent manner as results of dose-dependent toxicity mechanism and effects. Temporally dynamic

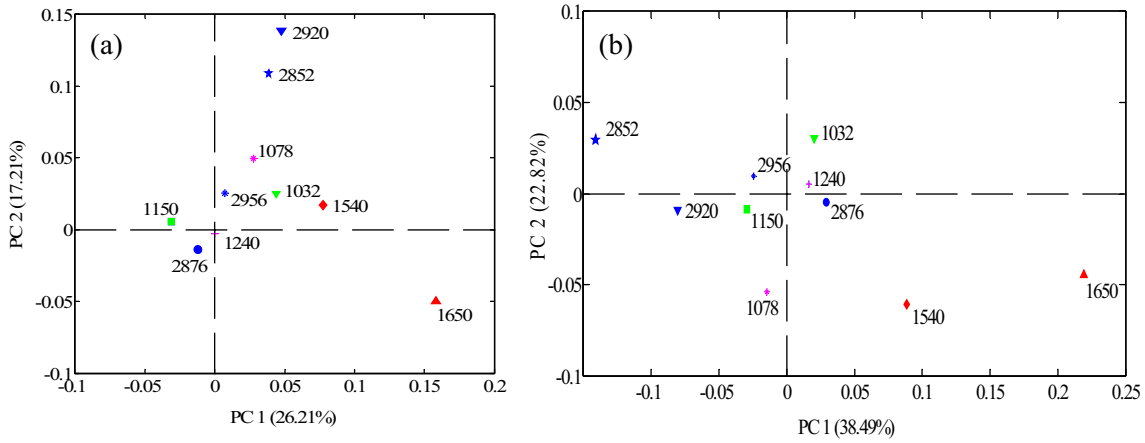

Fig. 3. Loading plots on PC1 vs. PC2 from principal component analysis performed over the region (3000–2700; 1800–750 cm^{-1}) of over 6000 FT-IR spectra obtained from samples exposed to $nTiO_2$ concentrations ranging from 1 to 1000 µg/L for 96 h (a) and 21 days (b). In red: proteins; in blue: lipids; in green: polysaccharides; in pink: nucleic acids. Details on band assignment are presented in STable 3.

and $nTiO_2$ concentration-dependent changes in the major cellular macromolecules, as indicated by the FT-IR fingerprints, were observed and they are further discussed in more details in the following sections.

3.4. Changes in cellular carbohydrates during $nTiO_2$ exposure

Dose-dependent temporal trends of carbohydrates/amide I ratios (Fig. 4) showed clear differences ($p < 0.06$) in the ratio value between those treated with $nTiO_2$ dose higher than 10 μg/L and untreated controls. The reduction in the carbohydrate/amide I ratio was most pronounced (>32%) with the highest $nTiO_2$ dose at 1000 μg/L during the first 96 hour exposure. Temporal variation of the carbohydrate/amide I ratio values was observed in all samples, including the control with no exposure, indicating that transitional and temporal cellular changes occur at initial exposure and self-recovering or adjustment to more stable conditions is achieved after a longer period of time (>10 days).

Except for a few exclusions, the average carbohydrate/amide I ratio found in this study is in the range of those reported in Dean et al. (0.25 to 0.82) (Dean et al., 2007). The carbon/protein ratios are sensitive indicators of algal chemical composition and rates of physiological processes, and provide insights into the adaptive response in the allocation of cell resources after exposure to pollutants or to generic conditions of stress (Geider, 1987). Dynamic reallocations of intracellular carbon into polysaccharides during regular growth of cyanobacteria (Carr and Whitton, 1982) and fluctuations after cell transfer to fresh media (Dean et al., 2008) have been observed before. These results showed consistently lower carbohydrate/amide I ratios in those treated with $nTiO_2$ (10–1000 μg-$nTiO_2$/L) than the control, suggesting likely lower carbohydrate (energy) content and/or storage capacity of cells under $nTiO_2$ stress than the controls. Phenomena of carbon re-allocation have been reported in a previous study where cyanobacteria cells were subjected to environmental perturbation (i.e., P limitation) and explained as a cell physiological need to survive stress (Sigee et al., 2007).

3.5. Changes in nucleic acids during $nTiO_2$ exposure

Two IR vibrations at 1078 cm^{-1} (ν P=O) and 1240 cm^{-1} (ν_{as} P=O) wavenumbers were assigned to nucleic acids, representing the symmetric stretching and asymmetric stretching (P=O) of the phosphodiester backbones of nucleic acids (DNA and RNA), respectively. The characteristic functional group of nucleic acids at 1078 cm^{-1} (ν P=O) was normalized to amide I (1078 cm^{-1}/amide I) and it showed dose-dependent changes upon $nTiO_2$ exposure with progressively decreasing values as dose concentration increased (Fig. 5a). Throughout the testing period, the average internal ratio of the (1078 cm^{-1}) to amide I was consistently lower in the cultures exposed to $nTiO_2$ at >10 μg/L than the control. The second identified asymmetric P=O functional group at 1240 cm^{-1} of phosphodiester backbones of nucleic acids did not show dose-dependent relations for most of the time points analyzed (data not shown). This suggests that functional groups of the same macromolecule (e.g., DNA) may respond differently to $nTiO_2$ action.

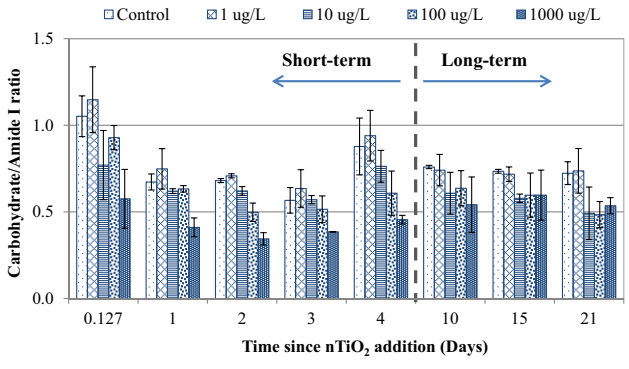

Fig. 4. Dose-dependent changes in the average carbohydrate/amide I ratio determined from 1032 cm^{-1} and 1650 cm^{-1} FT-IR vibration intensities for *A. variabilis* cells after exposure to different $nTiO_2$ concentrations ranging from 0 to 1000 μg/L, during short term (96 h) and long term (21 days) exposure. Standard deviations shown are calculated from biological duplicate experiments (n = 2). The carbohydrate/amide I ratio of each experiment was based on the average vibration intensity of the carbohydrate and amide I peaks collected from 60–80 spectra.

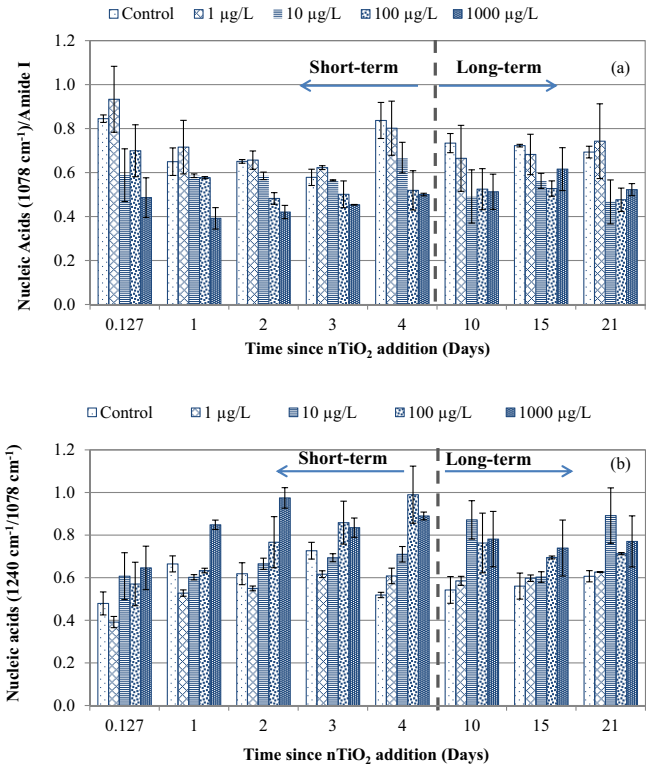

Fig. 5. Dose-dependent changes in the average nucleic acid (1078 cm^{-1})/amide I ratio (a) and average nucleic acid ratio (1078 cm^{-1}/1240 cm^{-1}) (b) determined from FT-IR vibration intensities for *A. variabilis* cells after exposure to different $nTiO_2$ concentrations ranging from 0 to 1000 μg/L, during short term (96 h) and long term (21 days) exposure. Standard deviations are calculated from biological duplicate experiments (n = 2). The nucleic acid/amide I ratio and the nucleic acid ratios (1078 cm^{-1}/1240 cm^{-1}) of each experiment were based on the average vibration intensity of the 1078 cm^{-1}, 1240 cm^{-1} and amide I peaks collected from 60 to 80 spectra.

Variations of the symmetric and asymmetric P=O vibrational modes and the fluctuation in their ratios (1240 cm^{-1}/1078 cm^{-1}, Fig. 5b) may reveal important insights into the potential mechanisms of the toxicant action. The alteration of the 1240 cm^{-1}/1078 cm^{-1} ratio has been previously reported in bacteria after exposure to ascorbic acid and linked to free radical generation (Melin et al., 2001). Our results may indicate that a similar effect is exerted by $nTiO_2$, which has been reported by us and others to generate reactive oxygen species and induce oxidative damage in cyanobacteria (Cherchi et al., 2011). In addition, shifts or intensity fluctuations of these stretching are often linked to the recognized binding potential of the phosphodiester bond with pollutants (D'Souza et al.; Li et al., 2010). Alterations in P=O modes are also believed to reflect changes in RNA cellular content (Chen et al., 2006), thus influencing important mechanisms of protein synthesis sustaining organisms' reproduction and growth (Gillooly et al., 2005). In addition, impairment of RNA allocation and cellular P content will more broadly impact the biogenesis of ribosomes, significant repository of P in ecosystems and intracellular element proportions, particularly associated to P-rich biomolecules (Li et al., 2010; Elser et al., 2003). In the long-term, this will have the potential to affect organisms' growth rate and fitness (Levin, 2009), and thus also biological productivity.

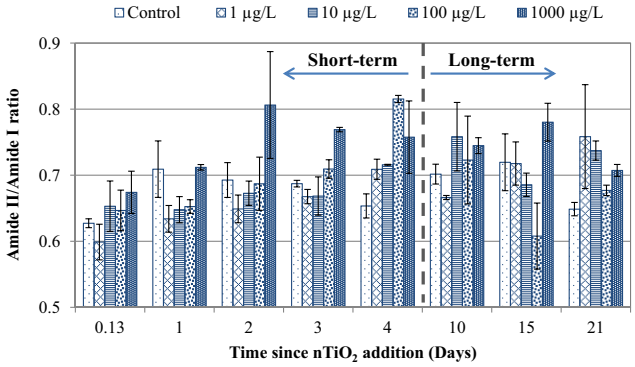

Fig. 6. Dose-dependent changes in the average amide II/amide I ratio determined from 1540 to 1650 cm^{-1} FT-IR vibration intensities for *A. variabilis* cells after exposure to different $nTiO_2$ concentrations ranging from 0 to 1000 μg/L, during short term (96 h) and long term (21 days) exposure. Standard deviations are calculated from biological duplicate experiments (n = 2). The amide II/amide I ratio of each experiment was based on the average vibration intensity of the amide II and amide I peaks collected from 60 to 80 spectra.

3.6. Changes in protein structure during $nTiO_2$ exposure

FT-IR allowed a finer-resolution examination of the potential protein pool structure and compositional changes. Fig. 6 shows the temporal changes in amide II/amide I ratio in all treatments, during both short and long term exposures. The highest $nTiO_2$ concentrations applied (1000 μg-$nTiO_2$/L) caused a significant increase ($p < 0.01$) of this ratio compared to the control by 0.4% (at day 1) to 16% (day 2), with an average of 10.6% increase during the other exposure times analyzed. In general, the relative increase of amide II with respect to amide I intensities indicates that conformational modifications in protein folding and unfolding, possible surface protein denaturation and changes in membrane protein secondary structure, are likely induced by $nTiO_2$ treatment during the initial exposure (Parikh and Chorover, 2006). Modifications of protein backbone conformation, such as secondary structure profiles and α- helix to β-sheet ratios may have important implications in cyanobacteria metabolism and response to stress, as well as protein internal utilization and availability (Yu, 2006).

3.7. Changes in lipids upon exposure to $nTiO_2$

Similar to the observation for carbohydrates over long-term exposure, although a temporal variation in the lipid/amide I ratio was observed for the first 96 h, a more conservative average value of the lipid/amide I ratio was obtained after 10 days for both treated and untreated cultures (data not shown). The final average ratio after 10 days seemed to decrease with increasing $nTiO_2$ doses, from 0.63 ± 0.01 in the control and 0.56 ± 0.04 and 0.42 ± 0.04 in the 1 and 10 μg/L exposures ($p < 0.04$), to 0.41 ± 0.02 and 0.44 ± 0.05 ($p < 0.003$) for treatments at 100 and 1000 μg-$nTiO_2$/L, respectively.

The comparison of the trends of lipid/amide I and carbohydrate/amide I ratios did not show any consistency or correlation, indicating that the dynamic trends are mostly due to variations in carbohydrate or lipids rather than modifications in the protein content alone. This is because if protein changes were responsible for the observed trend of the ratios of lipids/amide I and carbohydrates/amide I overtime, they would then correlate as suggested by Dean et al. (2008). These results suggest that $nTiO_2$ promotes changes in carbon allocation, decreasing both carbohydrate and lipid ratios. Alterations in the relative abundance of lipids caused by $nTiO_2$ exposure might also have contributed to *A. variabilis* structural changes (Cherchi et al., 2011). Changes in the asymmetrical $-CH_2$ vibrational frequencies caused by NM exposure were reported in recent studies, where Gram-positive and negative bacteria exposed to fullerenes showed dramatic changes in the conformational order of the membrane acyl chains (Fang et al., 2007).

4. Conclusions

In summary, chemical elemental analysis demonstrated $nTiO_2$-induced changes in cellular nutrient stoichiometry in *A. variabilis*, and further application of FT-IR analysis revealed cellular structure and composition (macromolecular ratios) alterations as results of $nTiO_2$ exposure at environmentally-relevant low doses (dose below those causing observable growth inhibition) on *A. variabilis*. The results indicated changes in intracellular stoichiometry of nutrients, such as in the decrease of C:N and concurrent increase in C:P and N:P ratios, and the PCA analysis based on FT-IR spectrum suggests possible potential reallocation of carbon among macromolecules and, particularly, from storage of C-rich products into proteins. The results demonstrated the pioneering application of FT-IR for physiological nanoecotoxicity investigations to reveal subtle intracellular effects such as the modifications in the intracellular pools of proteins and RNA-associated functional groups, energy storage products (i.e., carbohydrates and lipids), as well as the depository of genetic information (i.e., DNA). These findings imply an important warning that there might be long-term changes in the intracellular composition of ecologically relevant organisms at very low and environmentally relevant $nTiO_2$ concentrations (i.e., 1–100 μg-$nTiO_2$/L) and are interesting starting point for further studies. Primary producers' composition, in fact, affects food webs at all levels influencing their ability to thrive and to meet their nutritional requirements as previously discussed. This confirms the importance of understanding the effect of NMs on intracellular modifications of functionally key macromolecules, which can reflect changes at a larger scale involving community structures and dynamics in ecological systems.

Acknowledgments

This study was funded by grants from the National Science Foundation (EEC 0926284 and CAREER CBET 0953633, CBET 1440764), Center for High-rate Nanomanufacturing (CHN) seed grant from the Nanoscale Science and Engineering Centers Program of the National Science Foundation (Award # NSF-0425826). We are grateful to Professor Dhimiter Bello and his student Anoop Pal (Department of Work Environment, School of Health and Environment, University of Massachusetts Lowell, Lowell, MA) for providing the $nTiO_2$.

Appendix A. Supplementary data

SFig. 1 shows the growth inhibition of *A. variabilis* as a function of $nTiO_2$ dose concentrations for 21 day exposure. SFig. 2 shows time-dependent matrix plots of FT-IR spectra collected during *A. variabilis* growth. STable 1 summarizes the physical and chemical characterization of $nTiO_2$. STable 2 shows the correlation parameters of chlorophyll *a* and protein measurement with cell count of *A. variabilis* exposed to different $nTiO_2$ concentrations for 13 day exposure. STable 3 lists the FT-IR frequency band assignments for *A. variabilis*. Supplementary data associated with this article can be found, in the online version, at http://dx.doi.org/10.1016/j.scitotenv.2015.01.037.

References

American Public Health Association, 1999. Water Environment Federation Standard Methods for the Examination of Water and Wastewater. 22nd ed. American Water Works Assn.

Apte, S.K., Fernandes, T., Badran, H., Ballal, A., 1998. Expression and possible role of stress-responsive proteins in *Anabaena*. J. Biosci. 23 (4), 399–406.

Aruoja, V., Dubourguier, H.C., Kasemets, K., Kahru, A., 2009. Toxicity of nanoparticles of CuO, ZnO and TiO_2 to microalgae *Pseudokirchneriella subcapitata*. Sci. Total Environ. 407 (4), 1461–1468.

Augustin, C.B., Boersma, M., 2006. Effects of nitrogen stressed algae on different *Acartia* species. J. Plankton Res. 28 (4), 429–436.

Bello, D., Hsieh, S.F., Schmidt, D., Rogers, E., 2009. Nanomaterials properties vs. biological oxidative damage: Implications for toxicity screening and exposure assessment. Nanotoxicology 3 (3), 249–261.

Carr, N.G., Whitton, B.A., 1982. The Biology of Cyanobacteria. University of California Press, Berkeley and Los Angeles.
Chen, Y., Cheng, Y., Liu, H., Lin, P., Wang, C., 2006. Observation of biochemical imaging changes in human pancreatic cancer tissue using Fourier-transform infrared microspectroscopy. Chang Gung Med. J. 29 (5), 518–527.
Chen, J.Y., Dong, X., Zhao, J., Tang, G.P., 2009. In vivo acute toxicity of titanium dioxide nanoparticles to mice after intraperitioneal injection. J. Appl. Toxicol. 29 (4), 330–337.
Cherchi, C., Gu, A.Z., 2010. Impact of titanium dioxide nanomaterials on nitrogen fixation rate and intracellular nitrogen storage in *Anabaena variabilis*. Environ. Sci. Technol. 44 (21), 8302–8307.
Cherchi, C., Chernenko, T., Diem, M., Gu, A.Z., 2011. Impact of nano titanium dioxide exposure on cellular structure of *Anabaena variabilis* and evidence of internalization. Environ. Toxicol. Chem. 30 (4), 861–869.
D'Souza, L., Prabha Devi, D.S.M., Naik, C.G., 2008. Use of Fourier transform infrared (FTIR) spectroscopy to study cadmium-induced changes in *Padina tetrastromatica* (Hauck). Anal. Chem. Insights 3, 135–143.
Dean, A.P., Martin, M.C., Sigee, D.C., 2007. Resolution of codominant phytoplankton species in a eutrophic lake using synchrotron-based Fourier transform infrared spectroscopy. Phycologia 46 (2), 151–159.
Dean, A.P., Nicholson, J.M., Sigee, D.C., 2008. Impact of phosphorus quota and growth phase on carbon allocation in *Chlamydomonas reinhardtii*: an FTIR microspectroscopy study. Eur. J. Phycol. 43 (4), 345–354.
Eisbrenner, G., Distler, E., Floener, L., Bothe, H., 1978. The occurrence of the hydrogenase in some blue-green algae. Arch. Microbiol. 118 (2), 177–184.
Elser, J., 2006. Biological stoichiometry: a chemical bridge between ecosystem ecology and evolutionary biology. Am. Nat. 168 (6), S25–S35.
Elser, J.J., Acharya, K., Kyle, M., Cotner, J., Makino, W., Markow, T., Watts, T., Hobbie, S., Fagan, W., Schade, J., Hood, J., Sterner, R.W., 2003. Growth rate–stoichiometry couplings in diverse biota. Ecol. Lett. 6 (10), 936–943.
Fang, J.S., Lyon, D.Y., Wiesner, M.R., Dong, J.P., Alvarez, P.J.J., 2007. Effect of a fullerene water suspension on bacterial phospholipids and membrane phase behavior. Environ. Sci. Technol. 41 (7), 2636–2642.
Fernandes, T.A., Iyer, V., Apte, K., 1993. Differential responses of nitrogen-fixing cyanobacteria to salinity and osmotic stresses. Appl. Environ. Microbiol. 59 (3), 899–904.
Geider, R.J., 1987. Light and temperature dependence of the carbon to chlorophyll *a* ratio in microalgae and cyanobacteria: implications for physiology and growth of phytoplankton. New Phytol. 106, 1–34.
Geis, S.W., Fleming, K.L., Korthals, E.T., Searle, G., Reynolds, L., Karner, D.A., 2000. Modifications to the algal growth inhibition test for use as a regulatory assay. Environ. Toxicol. Chem. 19, 36–41.
Gillooly, J.F., Allen, A.P., Brown, J.H., Elser, J.J., del Rio, C.M., Savage, V.M., West, G.B., Woodruff, W.H., Woods, H.A., 2005. The metabolic basis of whole-organism RNA and phosphorus content. Proc. Natl. Acad. Sci. U. S. A. 102 (33), 11923–11927.
Giordano, M., Kansiz, M., Heraud, P., Beardall, J., Wood, B., McNaughton, D., 2001. Fourier transform infrared spectroscopy as a novel tool to investigate changes in intracellular macromolecular pools in the marine microalga *Chaetoceros muellerii* (Bacillariophyceae). J. Phycol. 37 (2), 271–279.
Glibert, P.M., 2012. Ecological stoichiometry and its implications for aquatic ecosystem sustainability. Curr. Opin. Environ. Sustain. 4 (3), 272–277.
Gou, N., Onnis-Hayden, A., Gu, A.Z., 2010. Mechanistic toxicity assessment of nanomaterials by whole-cell-array stress genes expression analysis. Environ. Sci. Technol. 44 (15), 5964–5970.
Heraud, P., Stojkovic, S., Beardall, J., McNaughton, D., Wood, B.R., 2008. Intercolonial variability in macromolecular composition in P-starved and P-replete *Scenedesmus* populations revealed by infrared microspectroscopy. J. Phycol. 44 (5), 1335–1339.
Jha, A.N., Reeves, J.F., Davies, S.J., Dodd, N.J.F., 2008. Hydroxyl radicals ((OH)–O•) are associated with titanium dioxide (TiO_2) nanoparticle-induced cytotoxicity and oxidative DNA damage in fish cells. Mutat. Res. Fund. Mol. M. 640 (1–2), 113–122.
Ji, J., Long, Z.F., Lin, D.H., 2011. Toxicity of oxide nanoparticles to the green algae *Chlorella* sp. Chem. Eng. J. 170, 525–530.
Kansiz, M., Heraud, P., Wood, B., Burden, F., Beardall, J., McNaughton, D., 1999. Fourier transform infrared microspectroscopy and chemometrics as a tool for the discrimination of cyanobacterial strains. Phytochemistry 52 (3), 407–417.
Kiser, M.A., Westerhoff, P., Benn, T., Wang, Y., Perez-Rivera, J., Hristovski, K., 2009. Titanium nanomaterial removal and release from wastewater treatment plants. Environ. Sci. Technol. 43 (17), 6757–6763.
Levin, S.A., 2009. The Princeton Guide to Ecology. Princeton University Press, Princeton, New Jersey.
Li, N., Ma, L.L., Wang, J., Zheng, L., Liu, J., Duan, Y.M., Liu, H.T., Zhao, X.Y., Wang, S.S., Wang, H., Hong, F.S., Xie, Y.N., 2010. Interaction between nano-anatase TiO_2 and liver DNA from mice in vivo. Nanoscale Res. Lett. 5 (1), 108–115.
Liang, Y., Beardall, J., Heraud, P., 2006. Changes in growth, chlorophyll fluorescence and fatty acid composition with culture age in batch cultures of *Phaeodactylum tricornutum* and *Chaetoceros muelleri* (Bacillariophyceae). Bot. Mar. 49 (2), 165–173.
Lin, D.H., Ji, J., Long, Z.F., Yang, K., Wu, F.C., 2012. The influence of dissolved and surface-bound humic acid on the adhesion and toxicity of TiO2 nanoparticles to *Chlorella* sp. Water Res. 46, 4477–4487.
Melin, A.M., Perromat, A., Deleris, G., 2001. Effect of radical attack on bacteria: an application of FT-IR spectroscopy. Appl. Spectrosc. 55 (1), 23–28.
Miller, R.J., Lenihan, H.S., Muller, E.B., Tseng, N., Hanna, S.K., Keller, A.A., 2010. Impacts of metal oxide nanoparticles on marine phytoplankton. Environ. Sci. Technol. 44 (19), 7329–7334.
Mueller, N.C., Nowack, B., 2008. Exposure modeling of engineered nanoparticles in the environment. Environ. Sci. Technol. 42 (12), 4447–4453.
Mulholland, M.R., Capone, D.G., 2001. Stoichiometry of nitrogen and carbon utilization in cultured populations of *Trichodesmium* IMS101: implications for growth. Limnol. Oceanogr. 46 (2), 436–443.
Murdock, J.N., Wetzel, D.L., 2009. FT-IR microspectroscopy enhances biological and ecological analysis of algae. Appl. Spectrosc. Rev. 44 (4), 335–361.
Neal, A.L., 2008. What can be inferred from bacterium–nanoparticle interactions about the potential consequences of environmental exposure to nanoparticles? Ecotoxicology 17 (5), 362–371.
Pal, A.K., Bello, D., Budhlall, B., Rogers, E., Milton, D.K., 2011. Screening for oxidative stress elicited by engineered nanomaterials: evaluation of acellular DCFH assay. Dose–Response 1–23.
Parikh, S.J., Chorover, J., 2006. ATR-FTIR spectroscopy reveals bond formation during bacterial adhesion to iron oxide. Langmuir 22 (20), 8492–8500.
Patel, S.A., Currie, F., Thakker, N., Goodacre, R., 2008. Spatial metabolic fingerprinting using FT-IR spectroscopy: investigating abiotic stresses on *Micrasterias hardyi*. Analyst 133 (12), 1707–1713.
Rai, A.K., Abraham, G., 1993. Salinity tolerance and growth analysis of the cyanobacterium *Anabaena doliolum*. Bull. Environ. Contam. Toxicol. 51 (5), 724–731.
Schwarzenberger, A., Sadler, T., Von Elert, E., 2013. Effect of nutrient limitation of cyanobacteria on protease inhibitor production and fitness of *Daphnia magna*. J. Exp. Biol. 216 (19), 3649–3655.
Sharma, V.K., 2009. Aggregation and toxicity of titanium dioxide nanoparticles in aquatic environment—a review. J. Environ. Sci. Health A 44 (14), 1485–1495.
Sigee, D.C., Bahram, F., Estrada, B., Webster, R.E., Dean, A.P., 2007. The influence of phosphorus availability on carbon allocation and P quota in *Scenedesmus subspicatus*: a synchrotron-based FTIR analysis. Phycologia 46 (5), 583–592.
U.S. Environmental Protection Agency, 2002. Short-term Methods for Estimating the Chronic Toxicity of Effluents and Receiving Waters to Freshwater Organisms. EPA-821-R-02-013, 4th ed. (Washington D.C.).
Wang, J.J., Sanderson, B.J.S., Wang, H., 2007. Cyto- and genotoxicity of ultrafine TiO_2 particles in cultured human lymphoblastoid cells. Mutat. Res. Genet. Tox. En. 628 (2), 99–106.
Wang, J.X., Zhang, X.Z., Chen, Y.S., Sommerfeld, M., Hu, Q., 2008. Toxicity assessment of manufactured nanomaterials using the unicellular green alga *Chlamydomonas reinhardtii*. Chemosphere 73 (7), 1121–1128.
Wiesner, M.R., Bottero, J.-Y., 2007. Environmental nanotechnology. Applications and Impacts of Nanomaterials. McGraw Hill.
Xu, A., Chai, Y.F., Nohmi, T., Hei, T.K., 2009. Genotoxic responses to titanium dioxide nanoparticles and fullerene in gpt delta transgenic MEF cells. Part. Fibre Toxicol. 6, 3.
Yu, P.Q., 2006. Synchrotron IR microspectroscopy for protein structure analysis: potential and questions. Spectrosc. Int. J. 20 (5-6), 229–251.